

ACCUMULATION AND EFFECTS OF SPACE CHARGE IN DIRECT CURRENT CABLE JOINTS. PART II: SPACE CHARGE DENSITY AND ELECTRIC FIELD DETERMINATION

LUCIAN VIOREL TARANU, PETRU V. NOTINGERH, CRISTINA STANCU

Key words: Dc cable joints, Cross-linked polyethylene, Ethylene-propylene rubber, Space charge, Electric field, Electrical conductivity.

Part II of the paper show the effect of temperature and electric field on the space charge accumulation (bulk and superficial charge) in direct current cable joints with Ethylene-propylene rubber/Cross-linked polyethylene insulation. The bulk charge was determined by using some electroacoustic pulses (the pulsed electroacoustic method (PEA)) and the superficial charge was determined experimentally - from the measured bulk charge -, as well as by computation - using the electrical conductivity and permittivity. The results show that both the electric field and the temperature increase the space charge values. Moreover, even after the voltage cancellation, there are residual charges that produce a residual electric field, whose values can be higher than the partial discharges and/or electrical treeing inception values.

1. INTRODUCTION

In [1], a model and two methods for computing the space charge densities (volume and superficial) were presented, as well as the variation with the temperature and electric field of the electric conductivities of the dc cable joint's insulation layers – respectively of cross-linked polyethylene (XLPE) and ethylene-propylene rubber (EPR). In this paper (Part II) the results of the bulk (experimentally) and superficial (experimentally and by computation) space charge densities determinations, as well as the resulting electric field – in the presence and in the absence of the voltage – are presented.

2. CHARGE DENSITY

Using the direct current (dc) electrical conductivity values determined in [1], the values of the space charge densities accumulated in cylindrical samples were determined, in the absence and presence of voltages of 25, 50, 75 and 100 kV at $\theta = 30, 50, 70, 80$ and 90°C . The increase of the voltage to the set value for each measurement was performed continuously in 2 s for 25 kV, 5 s for 50 kV, 10 s for 75 kV and 30 s for 100 kV, and the power-off was performed in 1 s for 25 kV, and, respectively, 2, 3 and 5 s for the other voltages.

2.1. VOLUME CHARGE

2.1.1. VOLTAGE ON

Figures 1 – 4 show the variations with time and coordinate r of the volume (bulk) space charge density (ρ_v) determined experimentally in EPR/XLPE cylindrical samples having the dimensions: $r_1 = 8 \text{ mm}$, $r_{12} = 11.7 \text{ mm}$ and $r_2 = 12.6 \text{ mm}$. It is found that, after applying the voltage, in the vicinity of the electrodes, charges of the same polarity as that of the electrode potential (Homocharges) are separated (Fig. 1), and in the volume of the samples, both positive and negative charges are separated (Bulk charges). On the other hand, the maximum values of the volume charge densities increase with the voltage application time (Figs. 1 and 2), less for lower voltages (25 kV) and more for higher voltages (75–100 kV).

For example, if t increases from 1 to 3600 s, in the points near the vicinity of surface S_1 (respectively, for

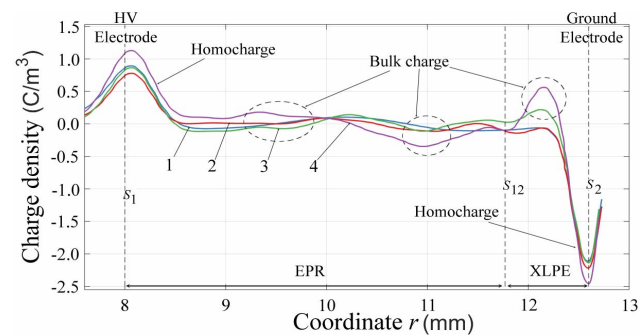


Fig. 1 – Variation of the volume space charge density with coordinate r , in EPR/XLPE, at different instants: 1 (1), 60 (2), 600 (3) and 3600 s (4) (Voltage On, $U = 100 \text{ kV}$, $\theta = 30^\circ\text{C}$).

$r = 8.2 \text{ mm}$), ρ_v increases 1.18 times for $U = 50 \text{ kV}$ and 1.29 times for $U = 100 \text{ kV}$.

These increases are explained by the increase in time of the injected charge from the electrodes compared to the one cancelled in the volume of the sample or at the electrodes [2].

Increasing the voltage applied to the samples leads to a significant increase in the charge density values ρ_v . This increase is lower for lower values of t , respectively immediately after Voltage On ($t = 1 \text{ s}$) and higher for higher values of t (Figs. 3 and 4).

These increases are mainly due to the increase in the concentration of charge carriers injected by the electrodes (e.g. by Schottky effect [2]), respectively electrons at the cathode and holes at the anode.

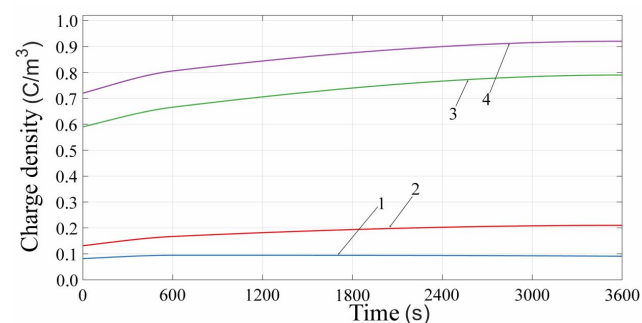


Fig. 2 – Variation of the volume space charge density with time, in EPR/XLPE, at points on the cylindrical surfaces of coordinate $r = 8.2 \text{ mm}$ (in the vicinity of the HV electrode), for $U = 25 \text{ kV}$ (1), 50 kV (2), 75 kV (3) and 100 kV (4) (Voltage On, $\theta = 30^\circ\text{C}$).

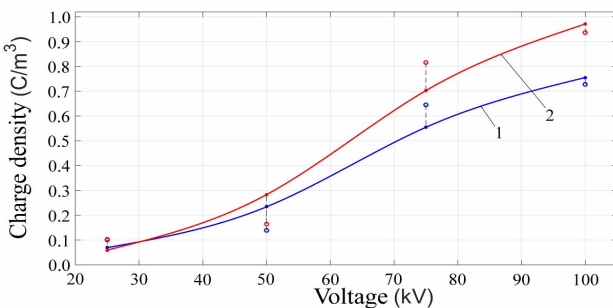


Fig. 3 – Variation of the volume space charge density (absolute values) with the voltage, in EPR/XLPE, at points on the cylindrical surface of coordinate $r = 8.2$ mm (in the vicinity of the HV electrode), at 1 (1) and 3600 s (2) (Voltage On, $\theta = 30^\circ\text{C}$).

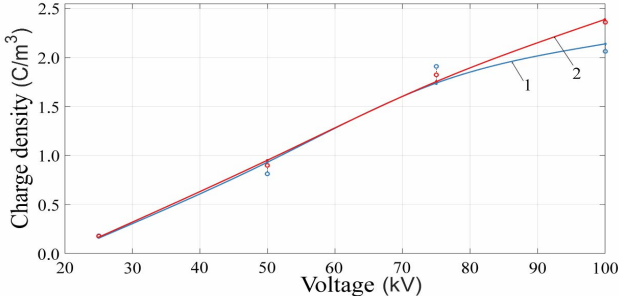


Fig. 4 – Variation of volume space charge density (absolute values) with the voltage, in EPR/XLPE, at points on the cylindrical surface of coordinate $r = 12.5$ mm, at 1 (1) and 3600 s (2) (Voltage On, $\theta = 30^\circ\text{C}$).

Thus, increasing the voltage from 25 to 100 kV causes an increase in the values of ρ_v of 7.1 times at $t = 1$ s and 9.29 times at $t = 3600$ s in the points in the vicinity of S_1 ($r = 8.2$ mm), and of 11.50 times at $t = 1$ s and 13.43 times at $t = 3600$ s in the points in the vicinity of the ground electrode ($r = 12.5$ mm).

2.1.2. VOLTAGE OFF

After voltage-off, the space charge density values and shapes modify, compared to those existing during Voltage On.

It is to be noticed that immediately after the voltage cancellation ($t = 1$ s), the curves $\rho_v(r)$ (Fig. 5, curve 1) have the same shape as those in the presence of the voltage (Fig. 1), the higher values of ρ_v corresponding to the higher applied voltage values (Fig. 6). On the other hand, the values of the charge density at the points in the neighbouring areas S_1 ($r = 8.2$ mm) and in particular S_2 ($r = 12.4$ mm) are considerably reduced over time (Figs. 5–7). For example, if t rises from 1 to 600 s, in the vicinity of S_2 , the ρ_v value decreases 5.5 times for $U = 50$ kV and 1.87 times for $U = 100$ kV (Fig. 8).

However, it should be noticed that ρ_v is not cancelled even after one hour from the disconnection of the voltage source, the higher values of ρ_v resulting for higher applied voltage values (Fig. 8).

2.2. SUPERFICIAL CHARGE

2.2.1. VOLTAGE ON

Changing the values of the electrical conductivity leads to the modification of the superficial charge density ($\rho_{s,cal}$) values on the S_{12} interface (Figs. 9 and 10). Thus, the computed values of $\rho_{s,cal}$ increase over time to a limit value $\rho_{s,l}$ (specific of each temperature) at which it stabilizes, after a certain time $\tau_{max,p}$. This increase happens very fast at

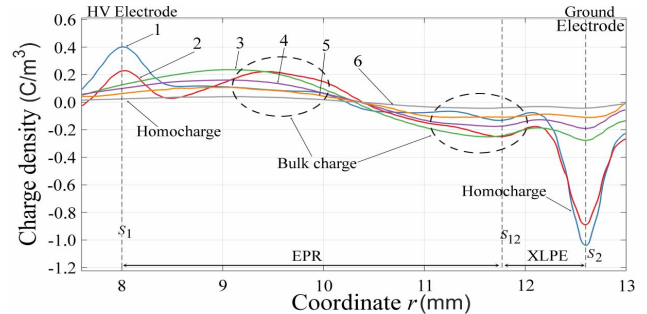


Fig. 5 – Variation of volume space charge density with the coordinate r , in EPR/XLPE, at $t = 1$ s (1), 60 (2), 600 s (3), 3600 s (4), 7200 s (5) and 10800 s (6) (Voltage Off, $U = 50$ kV, $\theta = 30^\circ\text{C}$).

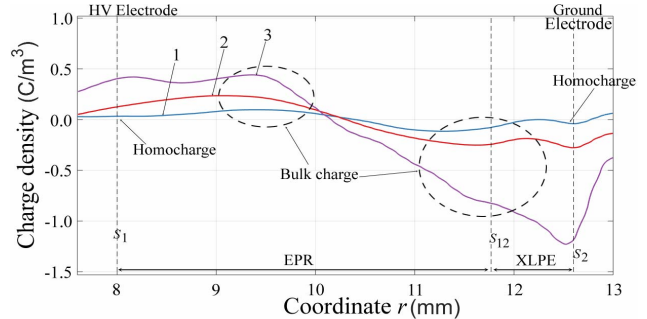


Fig. 6 – Variation the the volume space charge density with the coordinate r , in EPR/XLPE, at $t = 60$ s for $U = 25$ kV (1), 50 kV (2) and 100 kV (3) (Voltage Off, $\theta = 30^\circ\text{C}$).

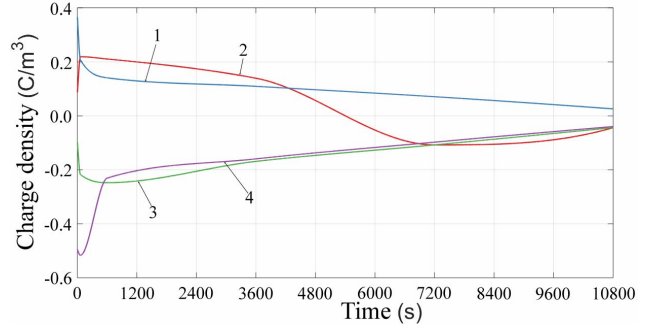


Fig. 7 – Variation with time of the volume space charge density at $r = 8.2$ mm (1), 9.5 mm (2), 11.5 mm (3) and 12.4 mm (4) (Voltage Off, $U = 50$ kV, $\theta = 30^\circ\text{C}$).

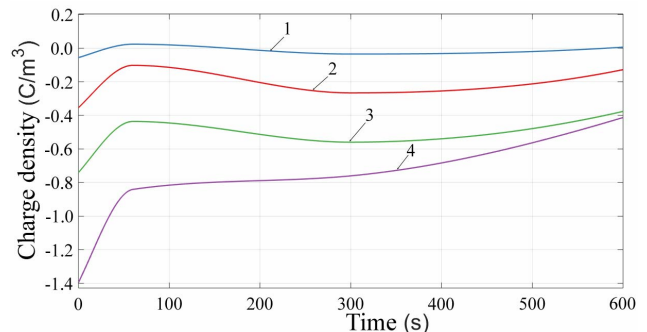


Fig. 8 – Variation with time of the volume space charge density near the ground electrode ($r = 12.4$ mm), for $U = 25$ kV (1), 50 kV (2), 75 kV (3) and $U = 100$ kV (4) (Voltage Off, $\theta = 30^\circ\text{C}$).

90°C (Fig. 9, curve 3) and much slower at temperatures close to room temperature (Fig. 9, curve 1). Increases of the superficial charge density with the temperature (Fig. 10) are mainly due to the increase of the values of the diffusion coefficient of the charge carriers with the

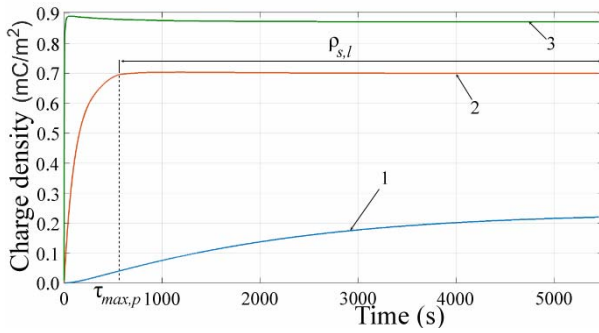


Fig. 9 – Variation with time of the calculated superficial charge density (absolute values) at the interface S_{12} , for $\theta = 30^\circ\text{C}$ (1), 60°C (2) and 90°C (3) (Voltage On, $U = 50\text{ kV}$).

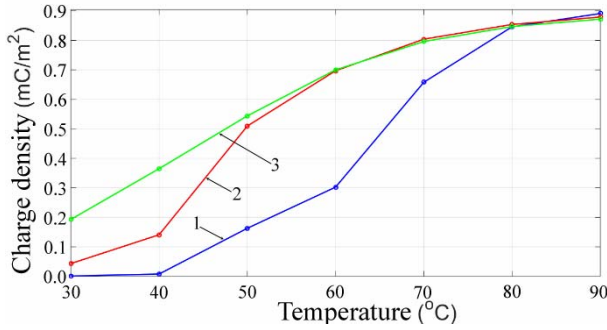


Fig. 10 – Variation with temperature of the calculated superficial charge density (absolute values) at the interface S_{12} , for $t = 60\text{ s}$ (1), 600 s (2) and 3600 s (3) (Voltage On, $U = 50\text{ kV}$, $\theta = 30^\circ\text{C}$).

temperature, respectively their mobility, both in EPR and XLPE.

The increase of $\rho_{s,l}$ is of great importance for cable joint operation. Thus, a higher value of $\rho_{s,l}$ leads to more important changes in the distribution of the electric field, especially to its intensification in certain areas, which makes easier the development of partial discharges and electrical trees, making easier the insulation failure [1]. On the other hand, the higher values of $\rho_{s,l}$ lead to the apparition of more intense residual electric fields, which facilitates the continuation of the electrical degradation processes of the insulation even after the cables are removed from operation.

Knowing the experimental values of ρ_v , the experimental values of ρ_s (respectively, $\rho_{s,exp}$) were determined with the equation (17), presented in [1]:

$$\rho_{s,exp} = \left(2 \int_{r_a}^{r_b} \rho_v(r) r dr \right) / (r_a + r_b) , \quad (1)$$

where r_a and r_b represent the radii of cylindrical surfaces very close together, located on both sides of the S_{12} interface (Fig. 3 in [1]).

The values of $\rho_{s,exp}$, determined at 30°C , for different voltages, are shown in Fig. 11. It is observed that, over time, the values of $\rho_{s,exp}$ increase as a result of the increase in the number of carriers displaced from the electrodes, this increase being more important for higher values of applied voltage, respectively for 100 kV (Fig. 11).

On the other hand, differences between the experimentally determined values $\rho_{s,exp}$ and calculated ones $\rho_{s,cal}$ ([1], equation (14)) can be seen, and that these

differences vary in time (Table 1). The relative difference between $\rho_{s,exp}$ and $\rho_{s,cal}$, denoted as ε_{rel} and defined with the equation :

$$\varepsilon_{rel} = |\rho_{s,exp} - \rho_{s,cal}| / \rho_{s,exp} , \quad (2)$$

has very low values for t close to 2400 s ($\varepsilon_{rel} \rightarrow 0$) and higher values immediately after applying the voltage and after reaching the steady state ($\varepsilon_{rel} \rightarrow 0.65$) (Table 1).

These differences are due, both, to measurement errors and to the approximation of the thickness of the interface, and to the computational hypotheses (homogeneous and isotropic environments, invariable permittivity with temperature and electric field, etc.).

2.2.2. VOLTAGE OFF

The variations in time of superficial charge density $\rho_{s,exp}$ determined experimentally after voltage cancellation are shown in Fig. 12. It is found that the values of $\rho_{s,exp}$ rise first (for a duration $\tau_{max,a}$) up to a maximum value $\rho_{s,exp,max}$.

Values of $\tau_{max,a}$ and $\rho_{s,exp}$ depend on the voltage values U , respectively $\tau_{max,a}$ and $\rho_{s,exp}$ increase with the voltage. It should be noted that the complete cancellation of ρ_s is not obtained even after 2 hours after the voltage-off.

If the time constant values after the superficial charge is stabilized (reaching $\rho_{s,l}$) are compared, respectively 50 kV Voltage On - $\tau_{max,p} = 5000\text{ s}$ ($\rho_s = 0.21\text{ mC/m}^2$) – Fig. 9 and Voltage Off - $\tau_{max,f} = 10000\text{ s}$ ($\rho_s = 0.1\text{ mC/m}^2$) – Fig. 12, it is found that the time constant value is 2 times higher after the Voltage Off (Fig. 12, curve 2) than from applying the voltage (Fig. 9, curve 1).

The duration of reaching the maximum value $\rho_{s,l}$ during Voltage On is lower than the value obtained during Voltage Off due to the increased electric fields established in the samples at the application of voltage (more intense as the applied voltage is higher).

Table 1
Superficial charge density values, determined experimentally $\rho_{s,exp}$ and computed $\rho_{s,cal}$ at different moments t from the voltage application (Voltage On, $U = 50\text{ kV}$, $\theta = 30^\circ\text{C}$)

t (s)	600	1200	2400	3600	5400
$\rho_{s,exp}$ (mC/m ²)	-0.1258	-0.1307	-0.1424	-0.1437	-0.1449
$\rho_{s,cal}$ (mC/m ²)	-0.0433	-0.0897	-0.1561	-0.1931	-0.2191
ε_{rel} (%)	65	31	9.6	34	51

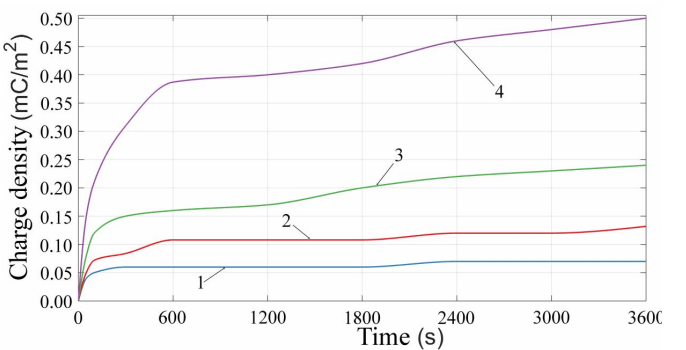


Fig. 11 – Variation with time of the experimental superficial charge density (absolute values) at the interface S_{12} , for $U = 25$ (1), 50 (2), 75 (3) and 100 kV (4) (Voltage On, $\theta = 30^\circ\text{C}$).

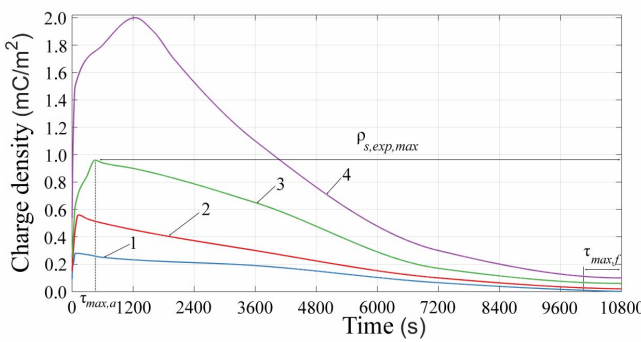


Fig. 12 – Variations with time of the experimental superficial charge density (absolute values) at the interface S_{12} , for 25 (1), 50 (2), 75 (3) and 100 kV (4) (Voltage Off, $\theta = 30^\circ\text{C}$).

3. ELECTRIC FIELD

3.1. VOLTAGE ON

For cylindrical samples with coordinates $r_1 = 8 \text{ mm}$, $r_{12} = 11.5 \text{ mm}$ and $r_2 = 12.6 \text{ mm}$, at temperatures between 30 and 90°C and for an applied voltage $U = 50 \text{ kV}$, the electric field values were computed at different moments from the voltage application ($t = 1 \dots 5500 \text{ s}$). A part of the results are shown in Figs. 13 – 20.

Figures 13 and 14 show the variations of the electric field E with the coordinate r in a sample at 30 , 60 and, respectively, 90°C , at four moments t after voltage application (1, 10, 60 and 600 s) computed in the absence of ρ_v , using the equations (15) and (16) (in [1]). It is found that, for any temperature value, E decreases with the increase of r and shows a sudden variation at the transition from EPR to XLPE. This is due, on one hand, to the reduction of the relative permittivity values (from 2.77 – for EPR - to 2.19 – for XLPE) ([1], Table 1), and, on the other hand, to the increase in the electrical conductivity values as the temperature increases (more in EPR and less in XLPE) ([1], [3–11]). Thus, when the temperature increases from 60 to 90°C , the electrical conductivity at the points adjacent to the S_{12} interface increases, for $t = 60 \text{ s}$, 6 times in EPR and 3.5 times in XLPE. Immediately after applying the voltage, at the points in EPR adjacent to the S_{12} interface there is an important increase in the electrical conductivity (see [1], Fig. 7), followed by a reduction of its values to the steady state. In the case of XLPE, in the first seconds there is a pronounced increase in conductivity (see [1], Fig. 8), followed by a slow increase when its values stabilize.

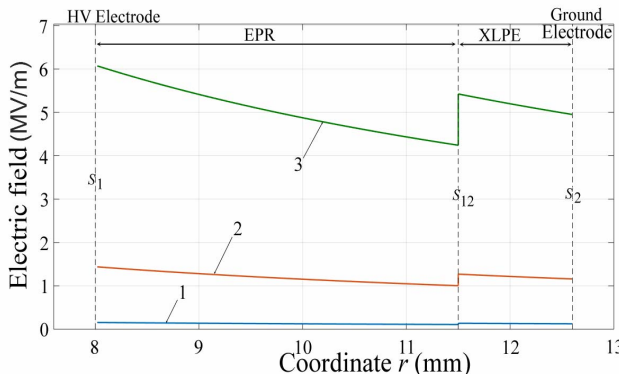


Fig. 13 – Variation with coordinate r of the electric field for $t = 1 \text{ s}$ (1), 10 s (2) and 60 s (3) (Voltage On, $U = 50 \text{ kV}$, $\theta = 30^\circ\text{C}$).

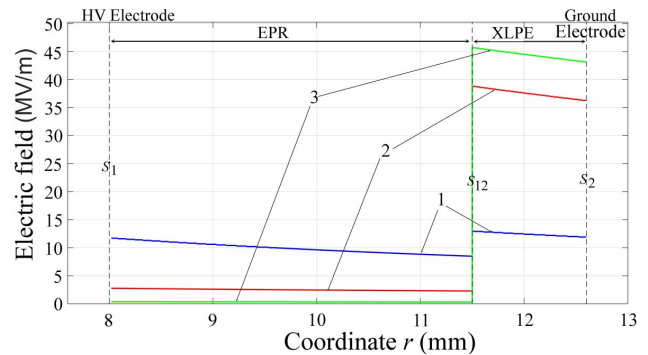


Fig. 14 – Variation with coordinate r of the electric field, for $\theta = 30^\circ\text{C}$ (1), 60°C (2) and 90°C (3) (Voltage On, $U = 50 \text{ kV}$, $t = 600 \text{ s}$).

The time variations of the electric field E in different areas of domain D , in the absence of volume charge density, are shown in Figs. 15 and 16. It is found that, in both subdomains, D_1 (EPR) and D_2 (XLPE), the electric field varies over time, but not in the same manner. Thus, in XLPE the field increases continuously: faster in the first 250 s and slower after 250 s (Fig. 15), and in the case of EPR, the electric field suddenly increases in the first 200 s, reaching a maximum value after approx. 500 s, then decreasing and stabilizes (Fig. 16). Depending on the temperature, the steady state is reached at different moments, as follows: in XLPE, after 3 h for 30°C and after 1 h for 60°C and 90°C and in EPR after 12 h for 30°C , after 2 h for 60°C and after 1 h for 90°C .

The variations of the electric field E with temperature at different points in the layers of EPR and XLPE are shown in Figs. 17 and 18. It is found that, after 3600 s, at all points in the EPR layer, the electric field decreases (for example, at the interface, E decreases about 15 times, when θ increases from 30 to 90°C), while in the XLPE layer, the electric field increases as the temperature increases (at the interface, E increases about 2.3 times, when θ increases from 30 to 90°C). These variations are mainly due to the significant increases in the conductivity values for the EPR layer [1, 4].

Figures 19 and 20 show the variation of the electric field with the temperature at the EPR/XLPE interface (S_{12}) for different time values. It is found that, in the case of higher temperature values (90°C), the field reaches the same steady-state regime, specific for each layer, respectively 0.3 MV/m for EPR (Fig. 19) and 45.5 MV/m for XLPE (Fig. 20), regardless of the duration of the voltage application (60 s or 3600 s).

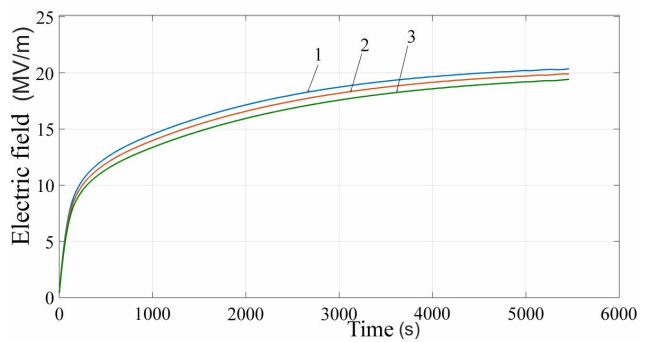


Fig. 15 – Variation with time of the electric field in XLPE, at coordinate $r = 11.5 \text{ mm}$ (1), 12 mm (2) and 12.6 mm (3) (Voltage On, $U = 50 \text{ kV}$, $\theta = 30^\circ\text{C}$).

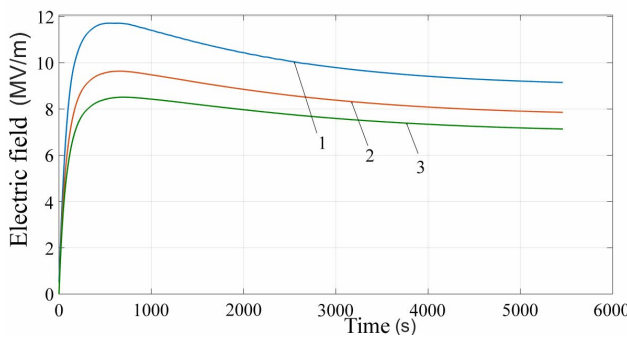


Fig. 16 – Variation with temperature of the electric field in EPR, at coordinate $r = 8$ mm (1), 9.75 mm (2) and 11.5 mm (3) (Voltage On, $U = 50$ kV, $t = 3600$ s, $\theta = 30^\circ\text{C}$).

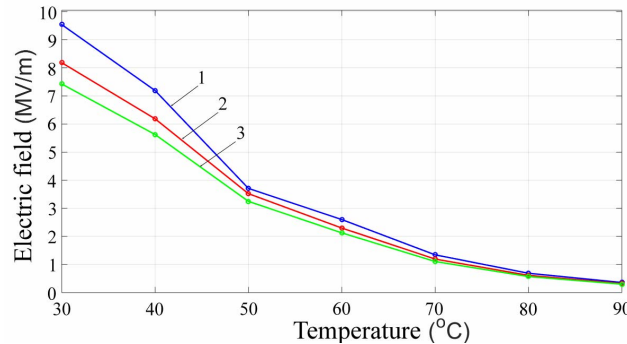


Fig. 17 – Variation with temperature of the electric field in EPR, at coordinate $r = 8$ mm (1), 9.75 mm (2) and 11.5 mm (3) (Voltage On, $U = 50$ kV, $t = 3600$ s, $\theta = 30^\circ\text{C}$).

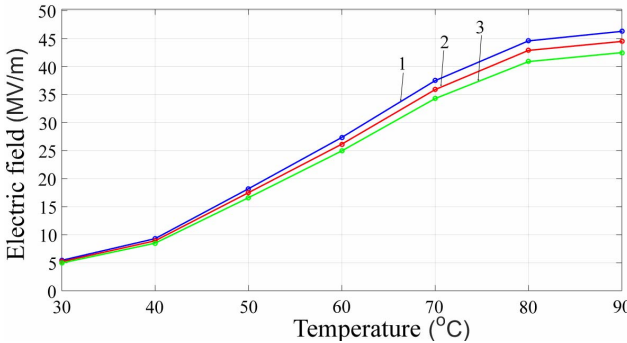


Fig. 18 – Variation with temperature of the electric field in XLPE, at coordinate $r = 11.5$ mm (1), 12 mm (2) and 12.6 mm (3) (Voltage On, $U = 50$ kV, $t = 3600$ s, $\theta = 30^\circ\text{C}$).

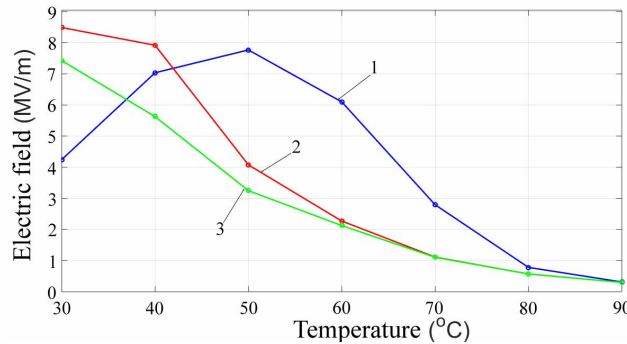


Fig. 19 – Variation with temperature of the electric field in EPR at the interface S_{12} , for $t = 60$ s (1), 600 s (2) and 3600 s (3) (Voltage On, $U = 50$ kV, $\theta = 30^\circ\text{C}$).

Variations of the electric field with coordinate r , in the presence of volume and superficial charges (on the S_{12} interface) at different moments from the Voltage On are shown in Fig. 21. It is found that the presence of space charge in the bulk of the sample reduces the electric field

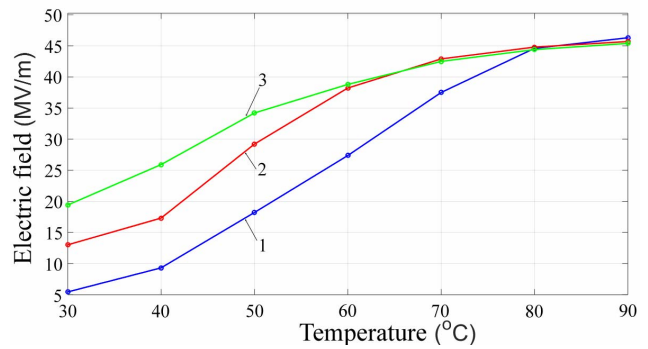


Fig. 20 – Variation with temperature of the electric field in XLPE at the interface S_{12} , for $t = 60$ s (1), 600 s (2) and 3600 s (3) (Voltage On, $U = 50$ kV, $\theta = 30^\circ\text{C}$).

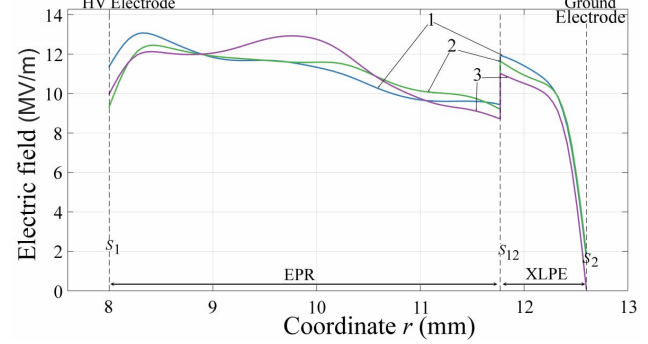


Fig. 21 – Variation with coordinate r of the electric field, in EPR/XLPE, at $t = 1$ s (1), 600 (2) and 3600 s (3) (Voltage On, $U = 50$ kV, $\theta = 30^\circ\text{C}$).

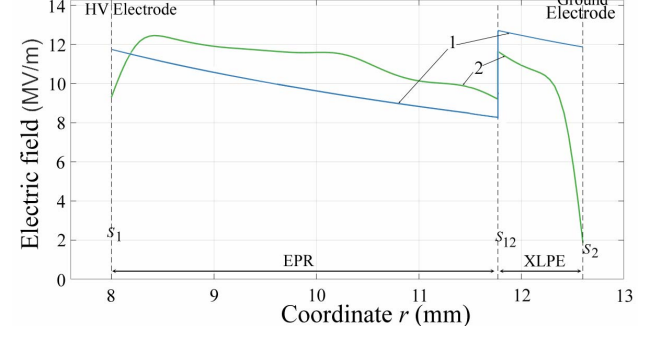


Fig. 22 – Variation with the coordinate r of the electric field at $t = 600$ s, in absence (1) and presence of volume space charge (2) (Voltage On, $U = 50$ kV, $\theta = 30^\circ\text{C}$).

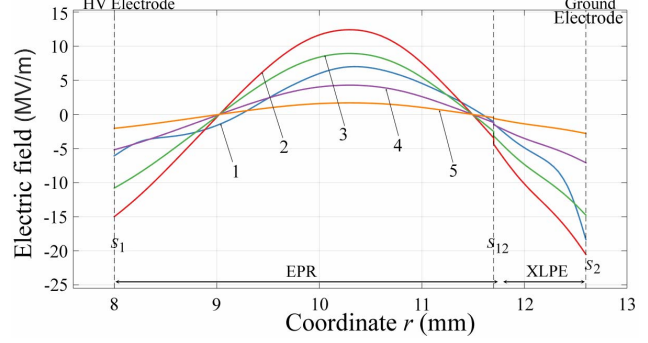


Fig. 23 – Variation with coordinate r of the electric field at $t = 1$ s (1), 600 (2), 3600 (3), 7200 (4) and 10800 s (5) (Voltage Off, $U = 50$ kV, $\theta = 30^\circ\text{C}$).

values in the vicinity of the electrodes, because they have the same signs as the electrodes potentials (homocharges, Fig. 5). Instead, the variations of E in the samples are different: E increases in EPR and decreases in XLPE (Fig. 22).

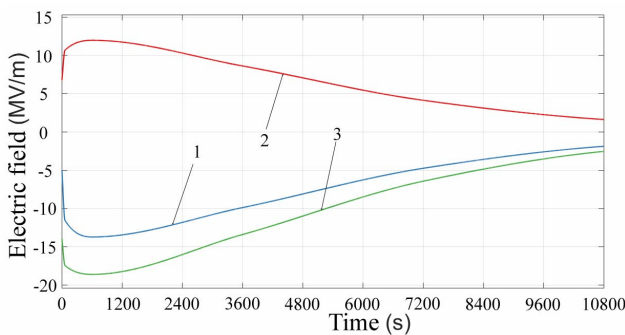


Fig. 24 – Variation with time of the electric field in points on the cylindrical surface with radius $r = 8\text{ mm}$ (1), 10.5 mm (2) and 12.6 mm (3) (Voltage Off, $U = 50\text{ kV}$, $\theta = 30^\circ\text{C}$).

3.2. VOLTAGE OFF

Figure 23 shows the variations of the electric field with coordinate r after Voltage Off for $U = 50\text{ kV}$ and $\theta = 30^\circ\text{C}$. It is found that after the voltage is cancelled, the electric field changes in the whole volume of the sample. Thus, its values decrease considerably, and in the vicinity of the electrodes the field changes its sign (Fig. 23, curve 1). On the other hand, field values change over time, respectively, increase in the first 10 minutes, and then decrease continuously, close to zero (Fig. 24). It should be noted the relatively important values of the electric field in the vicinity of the earth electrode, more than one hour after the voltage source (about 12 MV/m) is disconnected. As these residual fields (due to accumulated space charge) constitute, in the case of cable joints in service (and temporarily removed from power supply, for repair or maintenance work) important hazards, it is necessary that, for joints insulation, materials with lower space charge accumulation be used. For that purpose, the use of nanocomposites with different types of fillers is also recommended: ZnO [12], SiO_2 , TiO_2 [13], BaSrTiO_3 [14], MgO [15] etc.

4. CONCLUSIONS

The operation of power cables under continuous voltage leads to the accumulation of space charge in cable and joint insulations, both in the volume and at their interfaces. The charge density values depend on the nature and structure of the insulating materials, the magnitude and duration of the voltage application, etc.

The different values of the conductivities and electrical permittivity of EPR and XLPE determine the occurrence of a space charge at the EPR / XLPE interface, whose density varies with temperature and voltage applied to the insulation.

Connecting the conductor to the HV electrode at a positive potential leads to the apparition of homocharges in the vicinity of both electrodes during Voltage On.

The volume density of the accumulated charge in bi-layer insulations has two maxima in the vicinity of the electrodes, whose values increase with the voltage values.

The charge density values vary over time, *i.e.* they increase up to a limit value in the case of voltage application and tend to zero after its cancellation.

Increasing the temperature of the insulation causes an increase in the density of the space charge.

The accumulation of space charge modifies the distribution of the electric field in the joint insulation, in

certain areas the values of the field can greatly intensify.

After voltage power-off, a residual electric field remains inside the insulation whose values depend on the insulation characteristics, temperature and applied voltage values. As the applied voltage values increase, the accumulated charge and its related residual field take higher values.

ACKNOWLEDGEMENTS

The authors express their acknowledgement to ICME ECAB Bucharest and to the Laboratory of Innovation Technology (LIT) of the University of Bologna for technical support regarding the samples manufacturing and conductivity and space charge measurements.

Received on April 7, 2019

REFERENCES

1. L.V. Taranu, P. V. Notingher, C. Stancu, *Accumulation and Effects of Space Charge in Direct Current Cable Joints. Part I: Model and Methods for Space Charge Density Computation*, Rev. Roum. Sci. Techn.- Électrotechn. et Énerg., **64**, 2, 2019.
2. P. Notingher jr., *Etude de charge d'espace et des pertes dans l'isolant des câbles de transport d'énergie électrique en vue de l'accroissement du rendement*, PhD thesis, Université Montpellier II, 2000.
3. L.V. Taranu, P.V. Notingher, C. Stancu, *The Influence Of Electric Field And Temperature On The Electrical Conductivity Of Polyethylene For Power Cable Insulations*, U.P.B. Sci. Bull., **80**, 4, pp. 45–56, 2018, ISSN 1223-7027.
4. L.V. Taranu, P.V. Notingher, C. Stancu, *Dependence of Electrical Conductivity of Ethylene-Propylene Rubber on Electric Field and Temperature*, Rev. Roum. Sci. Techn. – Électrotechn. Et Énerg., **63**, 3, pp. 243–248, 2018, ISSN 0035-4066.
5. S. Boggs, D. H. Damon, J. Hjerrild, J. T. Holboll, M. Henriksen, *Effect of insulation properties on the field grading of solid dielectric DC cable*, IEEE Trans. Power Deliv., **16**, 4, pp. 456–461, 2001.
6. C. Stancu, P. V. Notingher, L. M. Dumitran, L. Taranu, A. Constantin, A. Cernat, *Electric field distribution in dual dielectric DC cable joints*, 2016 IEEE Int. Conf. on Dielectr. (ICD), pp. 402–405, 2016.
7. N. Adi, G. Teyssedre, T. T. N. Vu, N. I. Sinisuka, *DC field distribution in XLPE-insulated DC model cable with polarity inversion and thermal gradient*, 2016 IEEE Int. Conf. on HV Eng. and Applic. (ICHVE), pp. 1–4, 2016.
8. Z. Xu, W. Choo, G. Chen, *DC electric field distribution in planar dielectric in the presence of space charge*, 2007 IEEE Int. Conf. on Solid Dielectr., pp. 514–517, 2007.
9. O. L. Hestad, F. Mauseith, R. H. Kyte, *Electrical conductivity of medium voltage XLPE insulated cables*, 2012 IEEE Int. Symp. on Electr. Insul., pp. 376–380, 2012.
10. G. Jiang, J. Kuang, S. Boggs, *Evaluation of high field conduction models of polymeric dielectrics*, In: 2000 Annual Report Conf. on Electr. Insul. and Dielectr. Phenom. (Cat. No.00CH37132), pp. 187–190, 2000.
11. T. N. Vu, G. Teyssedre, B. Vissouvanadin, S. Roy, C. Laurent, *Correlating conductivity and space charge measurements in multi-dielectrics under various electrical and thermal stresses*, IEEE Trans. Dielectr. Electr. Insul., **22**, 1, pp. 117–127, 2015.
12. B. Du, J. Li, Z. Yang, *Nanocomposite for Space Charge suppression in HVDC Cable Accessory*, Nanocomposites - Recent Evolutions, 2019, ISBN: 978-1-78985-012-3.
13. I. Pleșa, P. V. Notingher, S. Schlögl, C. Sumederer, M. Muhr, *Properties of Polymer Composites Used in High-Voltage Applications*, Polymers, **8**, 173, pp. 1–63, 2016.
14. I. Pleșa, P.V. Notingher, C. Stancu, F. Wiesbrock, S.Schlögl, *Polyethylene Nanocomposites for Power Cable Insulations*, Polymers, **11**, 24, pp. 1–61, 2019.
15. A.M. Pourrahimi, L.K.H. Pallon, D. Liu, T.A. Hoang, S. Gubanski, M.S. Hedenqvist, R.T. Olsson, U.W. Gedde, *Polyethylene Nanocomposites for the Next Generation of Ultralow-Transmission-Loss HVDC Cables: Insulation Containing Moisture-Resistant MgO Nanoparticles*, ACS Appl. Mater. Interfaces, **8**, 23, pp. 14824–14835, 2016.